Int. J. Electrochem. Sci., 13 **(2018)** 7020 – 7033, doi: 10.20964/2018.07.40

International Journal of
ELECTROCHEMICAL
SCIENCE
www.electrochemsci.org

Carbon paper coated with Metal-free C-N electrocatalyst for Oxygen Reduction Reaction in Proton Exchange Membrane Fuel Cell

Chang Liu, Shang Li[*], *Yijing Xing, Huan Kang , Jinting Tan , Wei Guo, Mu Pan*

State Key Laboratory of Advanced Technology for Materials Synthesis and Processing, Wuhan University of Technology, Luoshi Road 122#, Wuhan 430070, PR China
[*]E-mail: lishang@whut.edu.cn

Received: 29 March 2018 / *Accepted:* 9 May 2018 / *Published:* 5 June 2018

Polyaniline (PANI) nanofibers were synthesized on carbon paper by electrochemical method, then heat-treated at temperatures of 800°C, 900°C, 1000°C and 1100°C to obtain a gas diffusion electrode (GDE). Fourier Transform infrared spectroscopy (FTIR), Scanning electron microscope (SEM), Transmission electron microscopy (TEM), X-ray diffraction (XRD) and X-ray photoelectron spectroscopy (XPS) were used to characterize the catalysts. The metal-free C-N catalyst with a reticular structure was coated on carbon paper. The ORR (oxygen reduction reaction) activity of metal-free C-N catalysts was evaluated by cyclic voltammetry (CV) and rotating disk electrode (RDE) in $HClO_4$. The results showed that the catalysts heat-treated at 1000°C had the best ORR activity and better stability compared with the commercial Pt-based catalysts in acidic medium. The result of XPS showed that the activity of metal-free C-N catalysts was related to the pyridinic-type nitrogen. Finally, the advantages and disadvantages of these catalysts were discussed for further investigation.

Keywords: Proton exchange membrane fuel cell (PEMFC), Metal-free catalyst, Electropolymerization, Oxygen reduction reaction

1. INTRODUCTION

In recent years, proton exchange membrane fuel cells (PEMFCs) are considered as a promising technology due to its high power density, high energy conversion efficiency, low local emissions and low operating temperatures [1]. However, the main drawback hampering PEMFC commercialization is the high cost of platinum-based catalysts. Therefore, the development of non-precious metal catalysts, which can reduce or even replace the platinum-based catalysts is a necessity [2].

Since the kinetics of the oxygen reduction reaction (ORR) on the platinum catalyst is slower and more complex than the hydrogen oxidation reaction (HOR) at the anode, the PEMFC cathode

requires more platinum catalysts. Thus, ORR is a dominant factor to evaluate the performance of fuel cell [2,3]. Nowadays, enormous efforts are made to study non-precious metal catalysts for the ORR on the cathode. Transition metal including transition metal oxides or nitrides, chalcogenides and macro-cycles (porphyrins or phthalocyanines) complexes are one of the promising alternatives [4-9]. Although the addition of transition metal species can enhance the performance of such type of catalyst, insufficient durability still remains one of the main barriers hindering their commercialization. The lack of durability is mainly caused by the leaching of transition metal ion such as Fe^{3+}, Co^{2+}, Cr^{3+} and their promoting effect on membrane degradation [10,11]. Some metal-free nitrogen-doped carbon catalysts such as nitrogen-doped carbon nanotubes [12,13], nitrogen-doped graphene [14,15] and nitrogen-doped ordered mesoporous carbon [16,17] have been investigated and showed good ORR activity. However, the synthesis of these catalysts includes the use of some metal catalysts . Therefore, it is difficult to ensure that there is no metal ion or residues in the final catalysts, since they cause some bad effects on the durability of MEA as mentioned above. However, the catalysts synthesized by an electrochemical method do not have any metal ions and it will not cause any fuel cell contamination.

A variety of approaches, such as optimization of heat-treatment temperature, conditions and synthesis procedure, investigation of different N-containing precursors, ligands and carbon supports materials, have been studied to improve the activity and stability of the nitrogen-doped carbon catalysts [18,19]. Nitrogen-containing precursors are very important in the synthesis of the nitrogen-doped carbon catalysts. Nitrogen containing precursors such as polypyrrole(Ppy), polyaniline(PANI), poly(3-methylthiophene) (P3MT), ethylenediamine, NH_3 and polyacrylonitrile have been recognized as effective nitrogen sources for the synthesis of the nitrogen-doped carbon catalysts [6-9,12-17,20-23]. PANI has been recognized as a promising precursor for nitrogen and carbon sources. Wu [6] reported the high ORR activity of doped carbon catalyst prepared from PANI-supported micro-porous carbon template incorporating cobalt and iron. The catalyst showed high ORR activity in an acidic medium (the ORR onset potential of the catalyst was 0.93 V vs. RHE.) and high stability for 700 hours in a long-term fuel cell performance test. Peng [24] reported a high ORR activity of Fe- and N-doped carbon catalyst with graphitic structure. The ORR onset potential of the catalyst was 0.98 V in 0.1 M $HClO_4$ solution and showed a great performance in a H_2-air single cell test (the maximum power density was 0.33 W cm^{-2} at 0.47 V).

PANI can be produced in different ways, which includes chemical polymerization, electrochemical polymerization, template and other methods. Comparing to other polymerization methods, electrochemical polymerization process has several advantages. Firstly, the initiation step and termination step can be controlled more easily [25]. Secondly, unlike the traditional chemical polymerization, reactions are more environmentally friendly and can reduce the pollution problem. Furthermore, PANI obtained by electrochemical polymerization is relatively pure because no additional chemicals, such as surfactant or oxidant are used in the synthesis process [26]. PANI nanostructures synthesized by electrochemical method, such as nanosheet, nanowire, nanoparticle and nanofiber are widely used in many areas due to their homogeneous morphology and high specific surface area. Wei [27] electropolymerized PANI/WO_3 nanocomposite films with a well crystallized nanocomposite structure. Moreover, the composite films showed an enhanced durability and had a great charge storage and discharge capacity after 1000 charge-discharge cycles. PANI helical

nanofibers with diameters of 80-110 nm synthesized via electrochemical method instead of template way also showed good electrochemical properties [28,29]. The electrochemical synthesis of PANI nanofibers includes galvanostatic method (GM), potentiostatic method (PM) and cyclic voltammetry (CV) method. Gupta [30] deposited PANI nanowires with the diameters ranging from 30~60 nm and the thickness of 20 μm on the 1×1 cm stainless-steel plates by using potentiostatical method. Zhang [31] used three different electrochemical methods (CV、GM、PM) to synthesize PANI nanofibers (mean diameter 50-150 nm) doped with $HClO_4$, which can be used as electrode materials for high-performance supercapacitor. However, the result showed that the PANI obtained by cyclic voltammetry method showed better electrical conductivity and homogeneity compared with the other two synthesis methods.

In this paper, electrochemical polymerization (cyclic voltammetry method) was used to prepare PANI nanofibers coated on carbon papers. Then compounds were heat-treated under different temperatures ranging from 800°C to 1100°C to obtain metal-free C-N catalysts. X-ray diffraction (XRD), Scanning electron microscope (SEM), Transmission electron microscopy (TEM) and X-ray photoelectron spectroscopy (XPS) were applied to analyze the composition, surface morphology and the structure and surface chemical composition of the catalysts. Fourier transform infrared spectroscopy (FTIR) was applied to characterize the structure of the PANI nanofibers and metal-free C-N catalyst. Raman spectroscopy was applied to analyze the structural defect of the catalysts. The electrochemical activities of the catalysts were examined using rotating disk electrode (RDE) techniques in acidic medium.

2. EXPRIMENTAL

2.1 Chemicals

Carbon paper was purchased from Wuhan WUT New Energy Co.,Ltd. Both $HClO_4$ and ethyl alcohol were purchased from Sinopharm Chemical Reagent Co., Ltd. (China). Aniline with purity of 99.9% was purchased from Aladdin Industrial Corporation. Nitrogen and Oxygen gases were supplied in cylinders with 99.999% purity. Commercial Pt/C catalyst (20 wt% Pt) was purchased from Johnson Matthey (UK). All reagents were of analytical grade and used as received without further purification. All solutions were prepared by using deionized water obtained from a Lab. deionized water filter system with a resistivity ≥18.25MΩ cm.

2.2 Catalyst preparation

The carbon paper was cleaned by ethyl alcohol and dried in an oven at 60°C for 2h. The electropolymerization of aniline were carried out using a conventional three-compartment electrochemical cell containing a working electrode (carbon paper), a counter electrode (Pt black electrode) and a reference electrode (a saturated calomel electrode (SCE)). To obtain PANI, a typical electrochemical polymerization was performed by 10 cycles scanned back and forth from 1 to 3 V vs.

SCE at a scan rate of 50 mV/s in 0.6 M $HClO_4$ aqueous solution containing 0.2 M aniline. Then the PANIs were dried in an oven at 60°C for 4 h. The PANI coated on carbon paper was placed in a tube furnace for 1 h under N_2 (99.999% purity) with a flow rate of 150 mL min^{-1} to remove any residual air before the desired heat-treatment temperature was increased. Then the tube furnace was adjusted to increase the temperature at a ramping rate of 5°C min^{-1} until the desired heat-treatment temperature reached, and was then held at this temperature for 2 h. The final metal-free C-N catalysts were obtained after the tube furnace was cooled down at a rate of 5°C min^{-1} to room temperature. The heat-treatment temperatures were 800°C, 900°C, 1000°C and 1100°C respectively. In this way, the final metal-free C-N catalysts were obtained and abbreviated as CN-800, CN-900, CN-1000, CN-1100 respectively.

2.3 Physical and surface characterization of the metal-free C-N catalysts

FTIR spectroscopy (Nicolet6700) was applied to characterize the structure of the prepared PANI and metal-free C-N catalyst. The morphology of the PANI and metal-free C-N catalyst samples were studied by using a Zeiss Ultra Plus scanning electron microscope (SEM) and JEM2100F transmission electron microscope (TEM). The structures of the catalysts were analyzed by XRD using D/Max-RB X-ray Powder Diffractometer with Cu-Ka radiation. The XRD patterns were recorded between 10° and 80° and a powder diffraction file database was used to assign the diffractograms. The electronic structure of the catalyst surface was analyzed by using XPS (ESCALAB 250Xi). The structural defects of the catalysts' surface were analyzed by using RENISHAW Raman microscope (INVIA).

2.4 Preparation of the working electrodes

The carbon paper coated with metal-free C-N catalyst was attached directly on glassy carbon (GC) disk electrode by 3μL Nafion® ionomer solution (5 wt%, Dupont). The geometric area of GC electrode was about 0.20 cm^2.

2.5 Electrochemical measurements

The electrochemical performances of the catalysts were carried out using a conventional three-compartment electrochemical cell in 0.1 M $HClO_4$ aqueous solution. The working electrode was a GC disk electrode coated with metal-free C-N catalyst. Platinum black electrode was used as the counter electrode and a saturated calomel electrode (SCE) was used as the reference electrode, which was calibrated against the reversible hydrogen electrode (RHE). Cyclic voltammogram (CV) was recorded by scanning the disk potential from -0.3 to 0.9 V vs. SCE at a scan rate of 50 mV s^{-1} in a nitrogen-saturated or oxygen-saturated $HClO_4$ solution. The ORR activity was carried out using RDE technique by linear sweep voltammetry (LSV) in the potential range of - 0.3 to 0.9 V (vs. SCE) at a scan rate of 5 mV s^{-1} in an oxygen-saturated $HClO_4$ solution. All current densities were normalized to the geometric

surface area of the disk electrode and all current densities reported in this paper were normalized to the RHE. All electrochemical experiments were carried out at a room temperature and ambient pressure.

2.6. Accelerated aging tests for catalysts

The stability of the metal-free C-N catalysts and Pt/C catalyst were evaluated by accelerated aging tests (AAT). Potential scans were carried out between - 0.3 to 0.9 V (vs. SCE) at a scan rate of 50 mV s^{-1} in an N_2-saturated aqueous solution of $HClO_4$ (0.1 mol L^{-1}). The electrochemical catalytic activities of the metal-free C-N catalysts and Pt/C catalyst before and after AAT were measured as aforementioned.

3. RESULTS AND DISCUSSION

3.1 FTIR analysis of the metal-free C-N catalysts

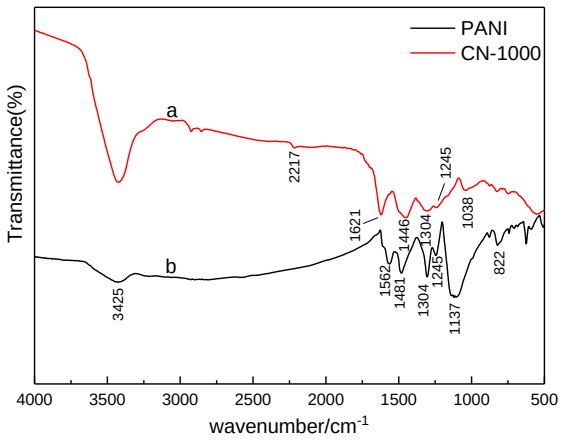

Figure 1. FTIR spectra of PANI and CN-1000

FTIR was used to characterize the structure of PANI before and after heat-treatment. Various bands of a typical PANI are shown in Fig. 1(b). The peaks at 822cm^{-1} and 1137 cm^{-1} represent the out-of-plane and in-plane bending of the C-H. The peaks at 1245cm^{-1} and 1304 cm^{-1} are assigned to C–N+• (polaron of PANI) and C–N stretching modes respectively. The peak at 1481 cm^{-1} and 1562 cm^{-1} are ascribed to C=C stretching mode of the benzenoid rings and quinoid respectively. These peaks are in good agreement with the FTIR spectrum of PANI in the previous reports [32,33], which indicate that the polymerization is successful. From the FTIR spectrum of CN-1000 (Fig. 1 (a)), it can be seen that after heat-treatment at 1000°C, the peaks at 822 cm^{-1} and 1137 cm^{-1} corresponding to the characteristic peaks of PANI gradually disappeared. The peaks at 1245 cm^{-1} and 1304 cm^{-1} weakened and

broadened, implying that the PANI had been carbonized and pyrolyzed after high-temperature heat treatment.

After heat-treatment, the peak of C=C stretching mode of the benzenoid rings shifted from 1481 cm^{-1} to 1446 cm^{-1}. We suppose that this is due to the heat-treatment resulting in the C=C bond getting longer, so the peak belonging to C=C shift to a lower wave. The new peak at 1621 cm^{-1} corresponds most probably to the presence of aromatic C=C stretching [34]. The peak at 2217 cm^{-1} is assigned to the nitrile group (C≡N). These spectra are almost similar to that of reported by Trchová [35]. The peak at 3425 cm^{-1} is ascribed to stretching vibrations of water molecules (OH^-) in the PANI and metal-free C-N catalyst. In summary, FTIR spectroscopy indicated the benzenoid rings are destroyed during the heat-treatment of 1000°C.

3.2 Morphology and structure of the metal-free C-N catalysts

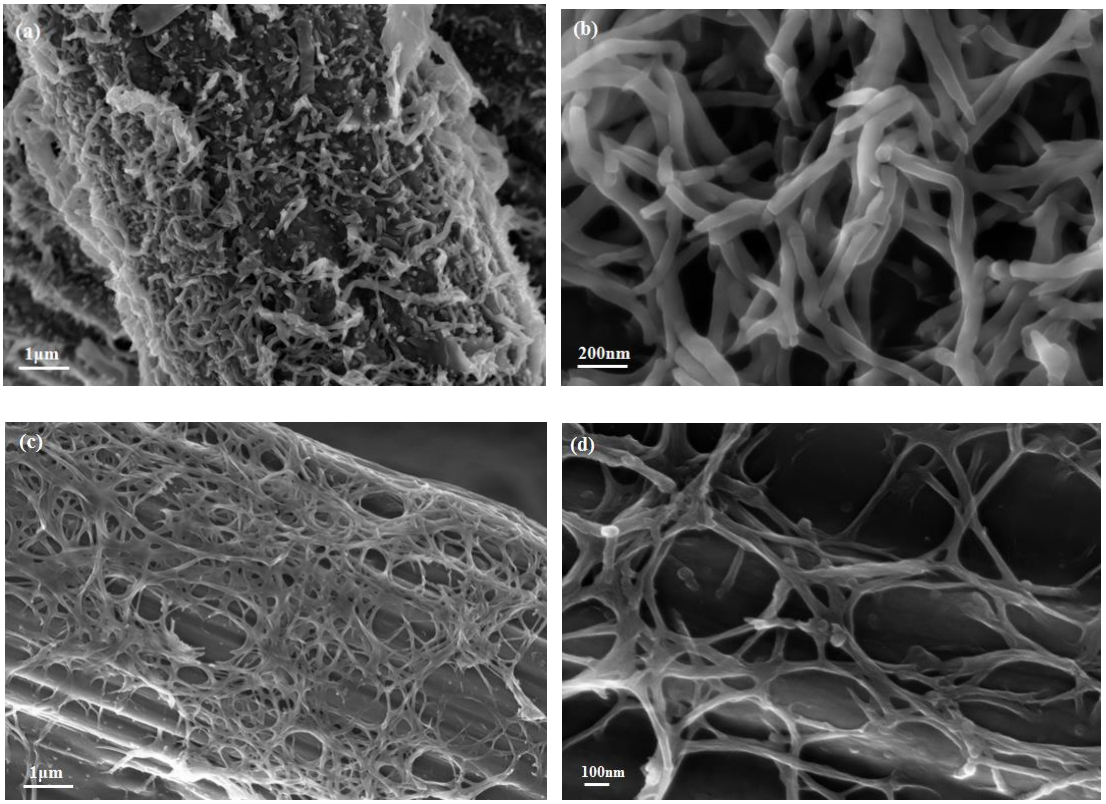

Figure 2. (a,b) SEM images of metal-free C-N catalyst before heat-treated at 1000°C (c,d) SEM images of metal-free C-N catalyst after heat-treated at 1000°C

The SEM and TEM images of PANI and metal-free C-N catalysts heat-treated at 1000°C are shown in Fig. 2 and Fig. 3 respectively. It can be seen from Fig. 2 (a), (b) that the PANI appears to be fibrous and the carbon fibers were wrapped with PANI nanofibers. Fig. 3(a) shows that the diameter of PANI nanofiber is about 80 ～ 120 nm before heat-treatment. Fig. 2 (c,d) and Fig. 3 (b) show the SEM and TEM images of CN-1000. The metal-free C-N catalysts are reticular and highly porous with interconnectivity, which laying on the surface of the carbon paper fiber uniformly, and the diameters

are about 40 ～70 nm. It is obviously that the diameter of PANI nanofiber becomes smaller after heat-treatment.

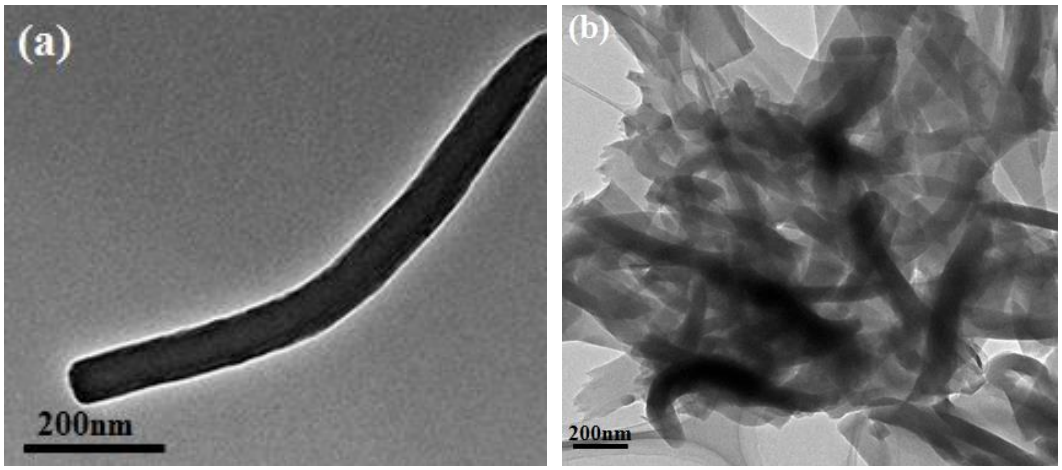

Figure 3. (a,b) TEM images of metal-free C-N catalyst before and after heat-treatment at 1000°C

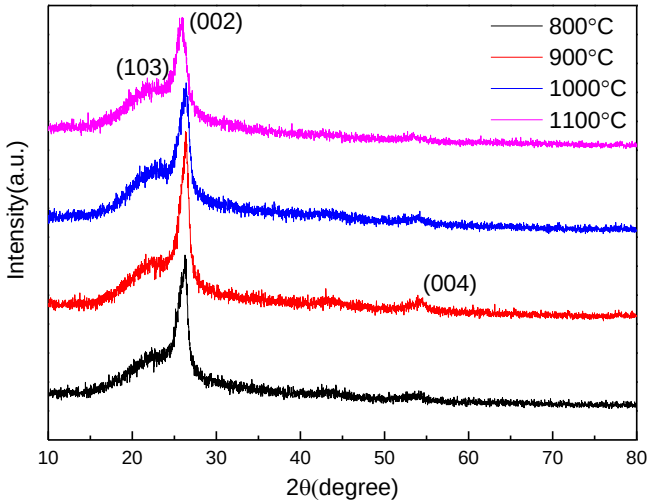

Figure 4. XRD patterns for metal-free C-N catalyst after being heat-treated at 800°C, 900°C, 1000°C and 1100°C

The XRD patterns of metal-free C-N catalyst obtained at different heat-treated temperatures are shown in Fig. 4. The wide peak at 24° corresponds to the amorphous carbon. The diffraction peaks at 2θ = 26.2° and 54° can be attributed to graphene-carbon (002) and (004) respectively, which are two types of allotropic crystalline form of carbon. The diffraction peaks at 2θ values of 26.2° slightly shifted to the left with the increase of temperature, which indicates the distortion of the crystalline regularity. Metallic diffraction peak was not observed, which confirms that these catalysts are indeed metal-free.

3.3 Catalytic ORR activity of the metal-free C-N catalysts

Fig. 5 shows the cyclic voltammogram of the metal-free C-N catalyst coated electrodes heat-treated at 1000°C, recorded in both N_2- and O_2-saturated 0.1 M $HClO_4$ solutions. For the N_2-saturated solutions, the reversible redox peaks appearing at 0.7 - 0.8 V vs. RHE correspond to the redox process of quinones (Eq. (1)) or the trace O_2 (Eq. (2)). The reduction wave near 0.4 V vs. RHE is generally attributed to the reduction reaction of O_2 (Eq. (3)), which may be derived from the trace solution of atmospheric O_2.

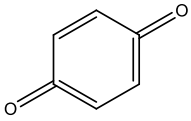

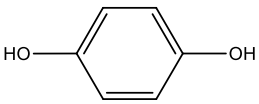

$+ 2H^+ + 2e^- \rightleftharpoons$ +0.6992 V (1)

$O_2(g) + 2H^+ + 2e^- \rightleftharpoons H_2O_2(aq)$ +0.70 V (2)

$O_2(g) + 2H_2O + 4e^- \rightleftharpoons 4OH^-(aq)$ +0.40 V (3)

In the presence of O_2, the reduction peak at 0.3 - 0.4 V vs. RHE changes greater, so it can be suggested that the metal-free C-N catalyst is active toward ORR in acidic electrolytes.

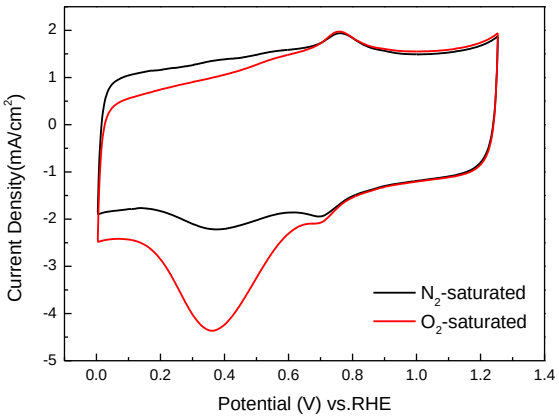

Figure 5. Cyclic voltammetry (CV) curves of metal-free C-N catalyst heat-treated at 1000°C. The catalyst was coated on a glassy carbon electrode surface. Recorded in N_2-saturated and O_2-saturated 0.1 M $HClO_4$ solutions. Potential scan rate: 50 mV s^{-1}.

3.4 Effect of heat-treatment temperature on the catalytic ORR activity of the metal-free C-N catalysts

Heat-treatment has an important effect on the ORR activity of the non-precious metal catalysts [18]. To optimize the heat-treatment temperature of the metal-free C-N catalysts, the liner scanning voltammetry (LSV) curves of the catalysts heat-treated at 800°C, 900°C, 1000°C and 1100°C in O_2-saturated $HClO_4$ were measured using rotating disk electrode (RDE) technique. Fig. 5 shows the ORR polarization curves of CN-800, CN-900, CN-1000 and CN-1100 respectively.

In accordance with Fig. 6, the polarization curves of metal-free C-N catalysts showed no plateau for limited current density in $HClO_4$. Judging from the onset potential, the order of catalytic activity is CN-1000>CN-900>CN-1100>CN-800. Among all the samples, the catalyst obtained at

heat-treatment temperature of 1000°C had the best ORR performance. Therefore, the catalyst obtained at 1000°C was used for all further studies. The onset potential was 0.816 V vs. RHE and the half wave potential was 0.54 V vs. RHE, which is similar to the result of heat-treated PANI-C catalyst in reference (synthesized by a chemical method) [6]. The mechanism for the effect of heat-treatment on ORR activity of the catalysts seems to be complicated and is not yet fully understood. It has been recognized that the main function of heat-treatment is to create active sites for the ORR [18].

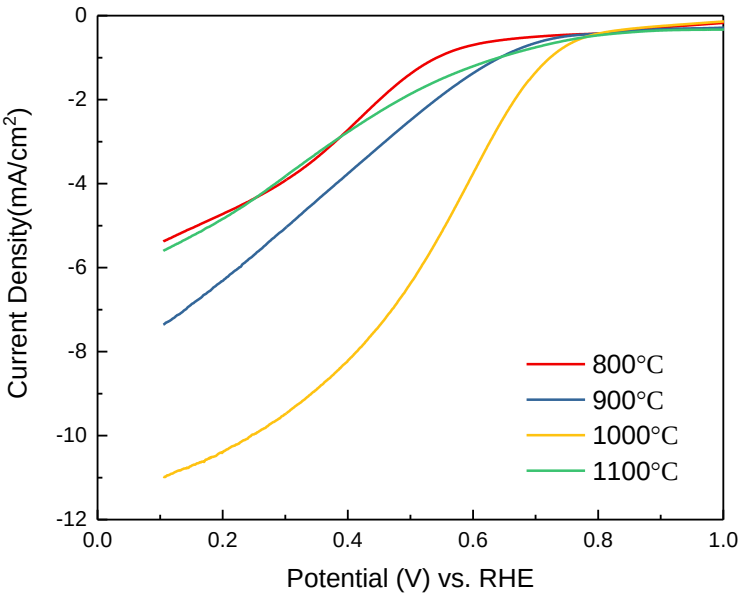

Figure 6. Current-voltage curves recorded on a rotating GC electrode coated with metal-free C-N catalyst heat-treated at various temperatures, as marked in the figure. Electrolyte: O_2-saturated 0.1 M $HClO_4$ solution; electrode rotating rate: 1600 rpm; potential scan rate: 5 mV s^{-1}.

3.5 Stability of the metal-free C-N catalysts

To evaluate the stability of the metal-free C-N catalysts, accelerated aging tests (AAT) were performed in 0.1M $HClO_4$ and compared to the commercial JM-20 wt% Pt/C catalyst. Fig. 7 shows the ORR curves of the metal-free C-N catalyst and JM-20 wt% Pt/C catalyst in 0.1 M $HClO_4$ before and after AAT. After 1000 cycles, the half-wave potential of CN-1000 decreased to 16 mV. In contrast, the JM-20wt% Pt/C exhibited a quick decrease, with a half-wave potential loss of 46 mV after 1000 cycles of AAT. This indicates that the metal-free C-N catalysts have much higher stability than Pt/C catalysts. The reasons may be the following: 1) The higher stability of metal-free C-N catalysts may be attributed to the nature of nitrogen doped active sites [37,38]. 2) The metal-free C-N catalysts do not have activity degradation caused by Pt nanoparticles agglomeration and loss such in the case of Pt/C when the successive potential cycling might cause the migration or aggregation of Pt nanoparticles and subsequent loss of the ORR catalytic activity [39].

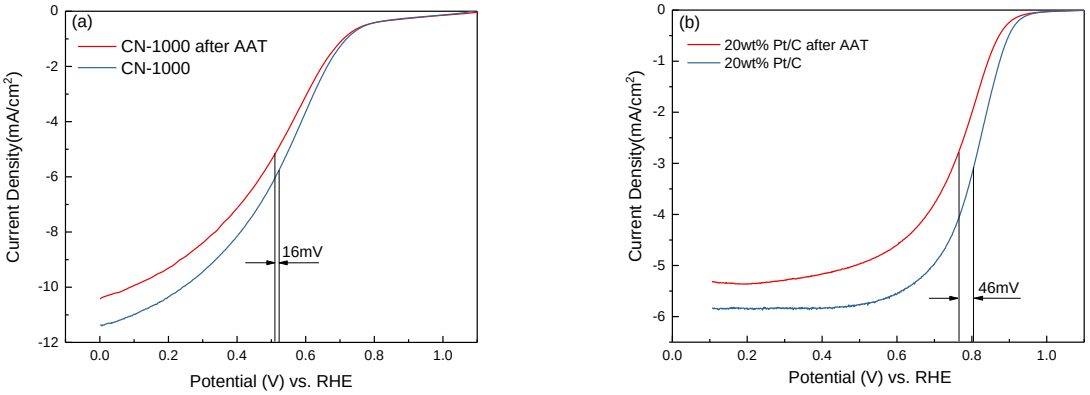

Figure 7. ORR Polarization curves before and after AAT (a) CN-1000, b) JM-20 wt% Pt/C. Electrolyte: O_2-saturated 0.1 M $HClO_4$ solution; electrode rotating rate: 1600 rpm; potential scan rate: 5 mV s^{-1}.

3.6 XPS analysis of the metal-free C-N catalysts

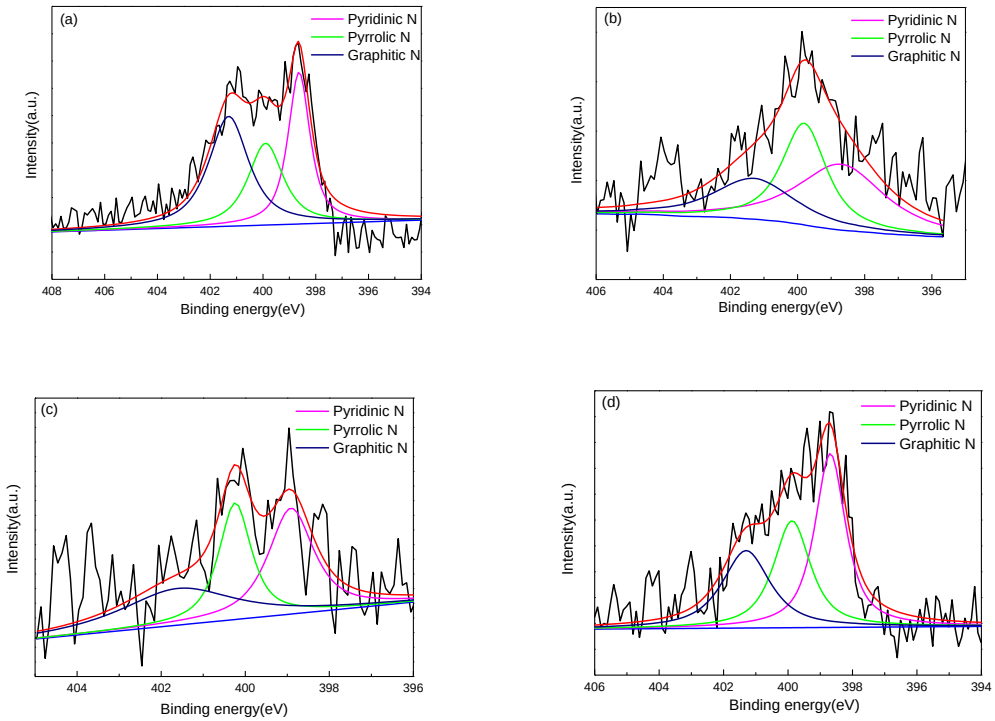

Figure 8. XPS narrow-scan spectra of (a) CN-800, (b) CN-900, (c) CN-1000 and (d) CN-1100

In order to analyze the mechanism for the effect of heat-treatment on ORR activity of the catalysts, XPS narrow-scan spectra of metal-free C-N samples heat-treated at 800°C, 900°C, 1000°C and 1100°C for N1s levels are shown in Fig. 8 and the N atomic nitrogen content is listed in Table 1.

The total nitrogen contents of metal-free C-N catalyst heat-treated at the temperature of 800°C, 900°C, 1000°C, 1100°C are about 2.46%, 2.01%, 2.31%, 1.89% respectively. Comparing to the results on Figure. 6, the total content of nitrogen is not proportional to the catalytic activity.

The XPS spectrum for the metal-free C-N catalysts after heat-treatment exhibited three nitrogen groups. The peak at 398.7 eV could be assigned to pyridinic N, which bonds with two carbon atoms on the edges of graphite planes with a basic lone pair of electrons [40]. The peak at 399.9 eV is due to the presence of pyrrolic N. Peaks at 401.3 eV can be attributed to graphitic N, which represents nitrogen atoms doped inside the graphitic carbon plane [41]. Details of the total nitrogen content and different types of nitrogen of the surface of the metal-free C-N catalysts are summarized in Table 1. It should be noted that the percentages of pyridinic N increased first and then decreased with the increase of heat-treatment temperature, CN-1000 had the highest piridinic nitrogen content. According to the recent studies, pyridinic nitrogen is considered to sinificantly increase the ORR activity [42,43]. As a consequence, the existence of pyridinic nitrogen in the metal-free C-N catalysts may be the superior active sites for ORR activities.

Table 1. The N atomic percentage of CN-800, CN-900, CN-1000, CN-1100

Heat-treated temperature(°C)	**Total N atomic(At.%)**	**Pyridinic N (At.%)**	**Pyrrolic N (At.%)**	**Graphitic N (At.%)**
800	2.46	0.77	0.67	1.02
900	2.01	0.80	0.78	0.44
1000	2.31	0.87	0.69	0.75
1100	1.89	0.78	0.57	0.54

3.7 Raman analysis of the metal-free C-N catalysts

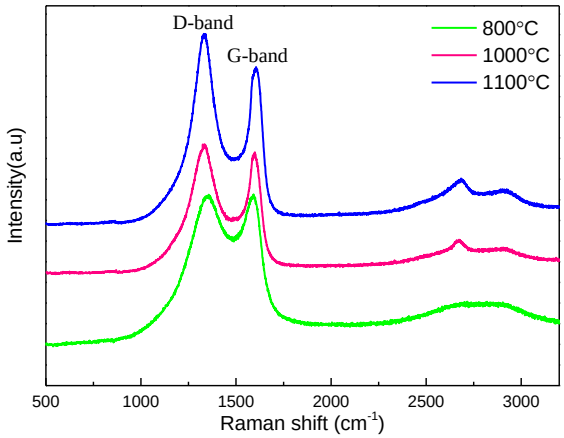

Figure 9. Raman spectra of metal-free C-N catalyst after being heat-treated at 800°C,1000°C and 1100°C.

Raman spectroscopy was used to analyze the structual defect of metal-free C-N catalysts. The peak at 1335cm^{-1} is the Raman active D band, which is attributed to structural defects and partially disordered structures of the sp^2 domains. The peak at 1596 cm^{-1} is the Raman active G band, which is attributed to the E_{2g} vibration mode present in the sp^2 bonded graphitic carbons [44]. The intensity ratio of the D band to G band (I_D/I_G) gives information of the degree of structral defects and a quantitative measure of edge plane explosure. Usually, higher I_D/I_G ratio indicates more defects present in the catalyst. Fig. 9 shows Raman spectra of CN-800, CN-1000 and CN-1100. The I_D/I_G ratio for CN-800, CN-1000 and CN-1100 are 1.00, 1.06, and 1.19 respectively. It can be seen that with the increase of the heat-treatment temperature, the I_D/I_G ratio shows an upward trend, which means there are more structural defects in the metal-free C-N catalyst. In addition, CN-1000 and CN-1100 appeared a peak at around 2674 cm^{-1} , which can be assigned to the 2D band. It is the most prominent feature of graphene in the Raman spectrum and its position and shape can be used to distinguish between single-layer, bilayer and few-layer graphenes [45]. Compared to metal-free C-N catalyst heat-treated at different temperature, it can be seen that the heat-treatment resulted in the formation of nanosheets structure (seen in SEM and TEM images).

3.8 Discussion

The ORR activity of metal-free C-N catalysts in this paper were lower than that of reference [6], which indicated that transition metal plays a significant role in the ORR activity of non-precious catalysts (M-N/C). However, for the fuel cells using M-N/C as cathode catalyst, in addition to the performance decreases caused by the loss of transition metal ions, the bad durability of fuel cell also comes from the existance of the transition metal ions (such as Co^{2+}, Fe^{3+}). These transitional metal ions may form a Fenton reagent with the H_2O_2 produced during oxygen reduction reaction process. Fenton reagent will highly accelerate the degredation of the resin in the catalyst layer and the proton exchange membrane [10,11]. Thus, the immobilization of Fe^{3+} and Co^{2+} will be an important research direction for the M-N/C catalyst.

Although the ORR activity of reticular metal-free C-N catalyst coated on carbon paper is lower than M-N/C, the stability is much better than commercial Pt/C catalyst. Moreover, the ordered porous structure catalyst layer grew directly on carbon paper can promote the transfer of O_2 and H_2O in PEMFC. This is a simple way to produce cheap and long-life gas diffusion electrode (GDE) by controlling the synthesis process, improving the ORR activity and adding ion exchange resin into the catalyst layer.

4. CONCLUSION

PANI nanofibers have been synthesized on carbon paper by electrochemical deposition method. The PANI nanofibers were heat-treated at the temperature of 800°C, 900°C, 1000°C and 1100 °C under N_2 to optimize their ORR activities. After heat-treatment, fibrous metal-free C-N

catalysts with reticular and highly porous structure were wrapped on the carbon paper. The catalyst heat-treated at 1000°C showed the highest ORR activity in acidic medium with an onset potential of 0.816 V vs. RHE and a half-wave potential of 0.54 V vs. RHE. The stability of the metal-free C-N catalyst was better compared to the Pt/C catalyst. The result of XPS indicated that pyridinic type nitrogen species played the most important role for ORR activity. This work developed a possible way to produce ordered porous catalyst layer on carbon paper direclty.

ACKNOWLEDGEMENTS
This work is supported by The National Key Research and Development Program of China (Program No. 2016YFB0101300 (2016YFB0101313)). We would like to thank Dr. Marina Shestakova of Lappeenranta University of Technology for proof-reading.

References

1. M. Miller, A. Bazylak, *J. Power Sources*, 196(2012)601.
2. F. Jaouen, E. Proietti, M. Lefèvre, R. Chenitz, J. Dodelet, G. Wu, T.C. Hoon, M.J. Christina and Z. Piotr, *Energ Environ Sci*, 4(2010)114.
3. L. Zhang, J. Zhang, D.P. Wilkinson and H. Wang, *J. Power Sources*, 156(2006)171.
4. N.A. Vante, W. Jaegermann, H. Tributsch, W. Hönle and Yvon. K, *ChemInform*, 109(1987)3251.
5. N. Alonso-Vante, H. Tributsch, O. Solorza-Feria, *Electrochim. Acta*, 40(1995)567.
6. G. Wu, K.L. More, C.M. Johnston and P. Zelenay, *Sci*, 332(2011)443.
7. C.W.B. Bezerra, L. Zhang, K. Lee, H. Liu, A.L.B. Marques, E.P. Marques, H. Wang and J. Zhang, *Electrochim. Acta*, 53(2008)4937.
8. S. Li, L. Zhang, H. Liu, M. Pan, L. Zan and J. Zhang, *Electrochim. Acta*, 55(2010)4403.
9. S. Li, L. Zhang, J. Kim, M. Pan, Z. Shi and J. Zhang, *Electrochim. Acta*, 55(2010)7346.
10. H. Li, J. Gazzarri, K. Tsay, S. Wu, H. Wang, J. Zhang, S. Wessel, R. Abouatallah, N. Joos and J. Schrooten, *Electrochim. Acta*, 55(2010)5823.
11. H. Li, K. Tsay, H. Wang, J. Shen, S. Wu and J. Zhang. *J. Power Sources*, 195(2010)8089.
12. K. Gong, F. Du, Z. Xia, M. Durstock and L. Dai, *Sci*, 323(2009)760.
13. Z. Chen, D. Higgins, H. Tao, R.S. Hsu and Z. Chen, *J. Phys. Chem. C*, 113(2009)21008.
14. Z.S. Wu, S. Yang, Y. Sun, K. Parvez, X. Feng and K. Müllen, *J. Am. Chem.Soc*, 134(2012)9082.
15. L. Qu, Y. Liu, J.B. Baek and L. Dai, *ACS nano*, 4(2010)1321.
16. G. Liu, X. Li, P. Ganesan and B.N. Popov, *Appl. Cata., B-Environ*, 93(2009)156.
17. K. Wan, G.F. Long, M.Y. Liu, L. Du, Z.X. Liang and P. Tsiakaras, *Appl. Catal., B-Environ*, 165(2015)566.
18. C.W.B Bezerra, L. Zhang, H. Liu, K. Lee, A.L.B Marques, E.P. Marques, H wang and J Zhang, *J. Power Sources*, 173(2007)891.
19. Z Chen, D. Higgins, A. Yu, L. Zhang and J. Zhang, *Energ Environ Sci*, 4(2011)3167.
20. C. Walter, K. Kummer, D. Vyalikh, V. Brüser, A. Quade and K.D. Weltmann, *J. Electrochem. Soc*, 159(2012)F560.
21. W. Feng, H. Li, X. Cheng, T.C. Jao, F.B. Weng, A. Su and Y.C. Chiang, *Appl. Surf. Sci*, 258(2012)4048.
22. E. Proietti, F. Jaouen, M. Lefèvre, N. Larouche, J. Tian, J. Herranz and J.P. Dodelet, *Nat. Commun*, 2(2010)109.
23. F. Jaouen, J. Herranz, M. Lefèvre, J.P. Dodelet, U.I. Kramm, I. Herrmann P. Bogdanoff, J Maruyama, T. Nagaoka, A. Garsuch, J.R. Dahn, T.Olson, S. Pylypenko, P. Atanassov and E.A. Ustinov, *Acs Appl. Mater. Interfaces*, 1(2009)1623.

24. H. Peng, Z. Mo, S. Liao, H. Liang, L. Yang, F. Luo, H. Song, Y. Zhong and B. Zhang, *Sci Rep*, 3(2013)1765.
25. X.Y. Peng, F. Luan, X.X. Liu, D. Diamond and K.T. Lau, *Electrochim. Acta*, 54(2009)6172.
26. S. Bhadra, D. Khastgir, N.K. Singha and J.H. Lee, *Prog. Polym. Sci*, 34(2009)783.
27. H. Wei, X. Yan, S. Wu, Z. Luo, S. Wei and Z. Guo. *J. Phys. Chem. C*, 116(2012)25052.
28. R. Li, Z. Chen, J. Li, C. Zhang and Q. Guo, *Synthetic. Met*, 171(2013)39.
29. S. Weng, Z. Lin, L. Chen and J. Zhou, *Electrochim. Acta*, 55(2010)2727.
30. V. Gupta, N. Miura, *Electrochem. Commun*, 7(2005)995.
31. Y. Zhang, G. Wang and M. Pan, *Chem. J. Chinese. U*, 35(2014)2234.
32. A. Kellenberger, E. Dmitrieva and L. Dunsch, *J. Phys. Chem. B*, 116(2012)4377.
33. Y. Li, X. Zhao, Q. Xu, Q. Zhang and D. Chen, *Langmuir*, 27(2011)6458.
34. L.L. Zhang, S. Zhao, X.N. Tian and X.S. Zhao, *Langmuir*, 26(2016)17624.
35. M. Trchová, P. Matějka, J. Brodinová, A. Kalendová, J. Prokeš and J. Stejskal, *Polym. Degrad. Stab*, 91(2006)114.
36. S. I. Tanuma, A. Palnichenko, *J. Mater. Sci. Lett*, 10(1995)1120.
37. P.H Matter, E Wang and Umit.S. O, *J. Catal*, 243(2006)395.
38. Y. M. Yu, J. H. Zhang , C. H. Xiao, J. D. Zhong, X. H. Zhang and J. H. Chen, *Fuel Cells*, 12(2012)506.
39. G. Mo, S. Liao, Y. Zhang, W. Zhang and J. Ye. *Electrochim. Acta*, 76(2012)430.
40. C.W.B. Bezerra, L. Zhang, K. Lee, H. Liu, J. Zhang, Z. Shi, A.L.B. Marques, E.P. Marques, S. Wu and J. Zhang. *Electrochim. Acta*, 53(2008)7703.
41. H.R. Byon, S. Jin and S.H. Yang, *Chem. Mater*, 23(2011)3421.
42. S. Kundu, T.C. Nagaiah, W. Xia, Y. Wang, S.V. Dommele, J.H. Bitter, M. Santa, G. Grundmeier, M. Bron, W. Schuhmann and M. Muhler, *J. Phys. Chem. C*, 113(2009)14302.
43. Z. Luo, S. Lim, Z. Tian, J. Shang, L. Lai, B. MacDonald, C. Fu, Z. Shen, T. Yu and J. Lin, *J. Mater. Chem*, 21(2011)8038.
44. K.N. Kudin, B. Ozbas, H.C. Schniepp, R.K. Prud'Homme, I.A. Aksay and R. Car, *Nano Lett*, 8(2008)36.
45. Z.H. Sheng, L. Shao, J.J. Chen, W.J. Bao, F.B. Wang and X.H. Xia, *Acs Nano*, 5(2011)4350.